JPE 19-3-5

https://doi.org/10.6113/JPE.2019.19.3.655
ISSN(Print): 1598-2092 / ISSN(Online): 2093-4718

Hopf Bifurcation Study of Inductively Coupled Power Transfer Systems Based on SS-type Compensation

Chenyang Xia†, Ying Yang*, Yuxiang Peng*, and Aiguo Patrick Hu**

†,*School of Electrical and Power Engineering, China University of Mining and Technology, Xuzhou, China
**Department of Electrical and Computer Engineering, University of Auckland, Auckland, New Zealand

Abstract

In order to analyze the nonlinear phenomena of the bifurcation and chaos caused by the switching of nonlinear switching devices in inductively coupled power transfer (ICPT) systems, a Jacobian matrix model, based on discrete mapping numerical modeling, is established to judge the system stability of the periodic closed orbit and to study the nonlinear behavior of Hopf bifurcation in a system under full resonance. The general flow of the parameter design, based on the stability principle for ICPT systems, is proposed to avoid the chaos and bifurcation phenomena caused by unreasonable parameter selection. Firstly, based on the state equation of SS-type compensation, a three-dimensional bifurcation diagram with the coupling coefficient as the bifurcation parameter is established with a numerical simulation to observe the nonlinear phenomena in the system. Then Filippov's method based on a Jacobian matrix model is adopted to deduce the boundary of stable operation and to judge the type of the bifurcation in the system. Then the general flow of the parameter design based on the stability principle for ICPT systems is proposed through the above analysis to realize stable operation under the conditions of weak coupling. Finally, an experimental platform is built to confirm the correctness of the numerical simulation and modeling.

Key words: Coupling coefficient, Full resonance, Hopf bifurcation, Inductively coupled power transfer (ICPT) system, Jacobian matrix

I. INTRODUCTION

With the progress of science and technology, the traditional power delivery method of transporting power with cables can no longer meet the increased requirements in terms of convenience, security and intelligence of the charging mode. This is due to the inevitable disadvantages of cables including unreliable contact, the hidden danger of naked conductors and poor flexibility of the power supply mode. Accordingly, wireless power transmission technology has emerged. Based on electromagnetic induction theory, inductively coupled power transfer (ICPT) systems, which are characterized by large power transmission capacity and high efficiency, have realized safe, reliable, efficient and flexible energy transmission without physical connections between the power supply lines and power equipment [1]-[4]. In addition, it has been widely studied in the fields of medical equipment [5], household appliances [6], electric car charging [7], mobile phone [8], etc.

Because of the switching of nonlinear switching devices, an ICPT system must be a time-varying strong nonlinear system. There may be phenomena like bifurcation, co-attractor and chaos when the system works under the conditions of weak coupling as well as unreasonable feedback control parameter design, which affect the system design [9],[10]. Although, linear analysis methods, such as impedance analysis [11], small signal modelling based on the state space average method [12], numerical method [13] and the generalized state space averaging method [14], can guide the design of a system to

Manuscript received Sep. 10, 2018; accepted Jan. 26, 2019
Recommended for publication by Associate Editor Fuxin Liu.
†Corresponding Author: bluesky198210@163.com
Tel: +86-18260722082, China University of Mining and Technology
*School of Electrical and Power Engineering, China University of Mining and Technology, China
**Department of Electrical and Computer Engineering, Faculty of Engineering, The University of Auckland, New Zealand

© 2019 KIPE

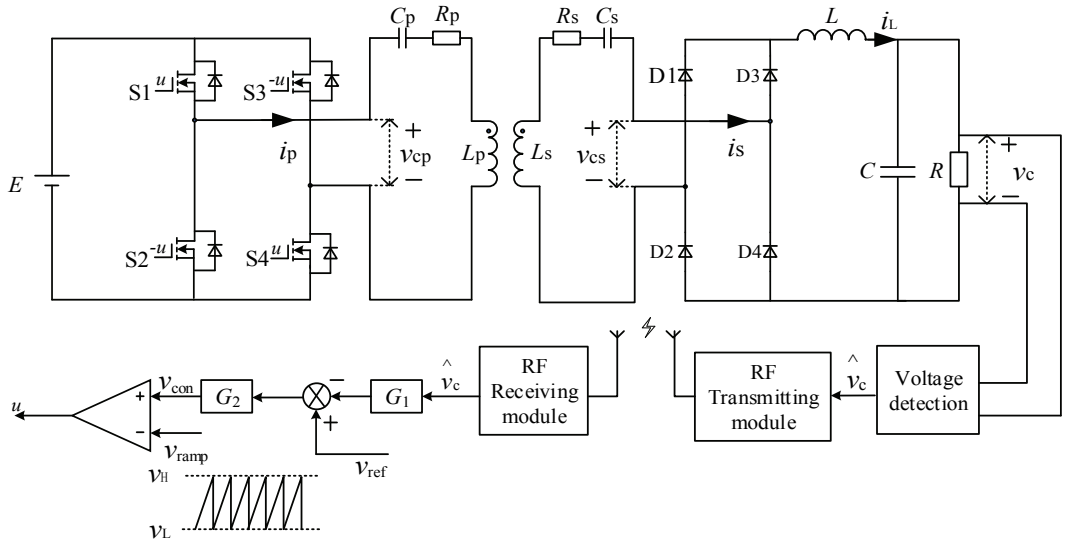

Fig. 1. Structure diagram of an ICPT system.

some extent, there are some disadvantages such as inaccurate modelling results and analysis of only the steady state behavior. Therefore, there is a need to adopt discrete mapping numerical modeling to study the nonlinear phenomena in ICPT systems.

At present, deep studies on the bifurcation and chaos of power electronic converters have been reported. A number of relatively accomplished methods has been studied for the bifurcation and chaos phenomena in different types of power electronic converters. Examples of this include analyzing low dimensional DC/DC converters with a small signal model or discrete mapping model, and estimating the stability of the system by calculating a Jacobi matrix eigenvalue [15]; analyzing the fast-scale bifurcation in a power factor correction (PFC) converter with discrete modelling, and determining the stability of the system by a Jacobi matrix eigenvalue [16]; analyzing the multi-scale and slow-scale bifurcation in PFC converters with an average modelling, and studying the system stability by the harmonic balance method and Floquet theory[17]; and analyzing the multi-scale and fast-scale bifurcation in a voltage-type full-bridge inverter with an average method and a discrete method, as well as estimating the stability of system by a Jacobi matrix eigenvalue [18]. However, a few studies have been made on the bifurcation and chaos in ICPT systems, despite the fact that there are already many achievements in DC-DC converters. Although the authors of [10] analyzed nonlinear phenomena in an ICPT system based on a loose coupling transformer model, the stability criterion of the system has not been deduced. As a result, it is not possible to confirm the type of bifurcation or verify the causes of the low-frequency oscillation.

In order to study the nonlinear phenomena in ICPT systems, a three-dimensional bifurcation diagram with the coupling coefficient as the bifurcation parameter is established with a numerical simulation to verify that the ICPT system does generate the nonlinear phenomena of bifurcation and chaos when nonlinear switching devices switch. Based on this assumption, a model is established to study the stability of the system and to calculate the stable operation boundary of the bifurcation parameter. Specifically, the ICPT system, characterized by autonomous segmental oscillation, is analyzed with discrete mapping numerical modeling and Filippov's method [19] to deduce a Jacobian matrix model. Then the eigenvalue of the Jacobian matrix is calculated to predict the boundary of stable operation and the position of the bifurcation point of the system. Then the general flow of the parameter design is proposed based on the stability principle of the ICPT system to realize stable operation under reasonable parameters. Finally, an experimental platform is built to study waveforms of the capacitor voltage and inductor current under a typical coupling coefficient to verify the correctness of the numerical simulation and modeling.

II. Structure and Working Modal Analysis of an ICPT System Based on SS-type Compensation

ICPT systems based on SS-type compensation have been widely studied in a number of applications since its structure is simple and its resonant network characteristics do not change with the load resistance. However, in actual systems, due to the existence of conductor inductance and other parasitic inductances, the capacitor filter circuit usually turns into an inductor-capacitor filter circuit. Therefore, this part of the parasitic inductance is expressed as L in the circuit. The structure of an SS-type compensation ICPT system is shown in Fig. 1. It is mainly composed of a DC power supply, an inverter circuit, primary and secondary resonance compensation circuits, a magnetic coupling mechanism, rectifying and filtering circuits, a load, a wireless communication module

TABLE I
SWITCHING STATES OF FULL-BRIDGE RESONANT CONVERTER

State	1	2	3	4	5	6
S1	on	on	off	off	on	off
S2	off	off	on	on	off	on
D2	on	off	off	on	off	off
D1	off	off	on	on	off	off
v_{con} & v_{ram}	>	>	<	<	>	<
i_s	>	<	<	>	=	=

and a PWM signal generation circuit. In Fig. 1, the primary and secondary resonance compensation adopt both series resonance compensation.

In this figure, E is the input DC voltage source. The MOSFETs S1, S2, S3 and S4 form the full-bridge inverter circuit. C_p and C_s are the primary and secondary resonant capacitors, respectively. L_p and L_s are the primary and secondary coil inductance, respectively. M is the coupled inductor between the primary and secondary coils. R_p and R_s are the parasitic resistances of the primary and secondary coil inductors, respectively. The diodes D1, D2, D3 and D4 form the rectifier circuit. L and C form the filter circuit. R forms the load.

To simplify the analysis, it is assumed that the system works at full resonance. In other words, the primary and secondary sides resonate separately and have the same frequency. At this time, the coupling coefficient of the primary and secondary sides of the system is:

$$k = \frac{M}{\sqrt{L_p L_s}} = \frac{M}{L_p} = \frac{M}{L_s} \tag{1}$$

The working process is that the output voltage of the secondary side is sampled and then transmitted to the primary side through wireless communication technology. To control the switch tube, the signal v_{con}, adjusted by the proportional ring, is compared with the sawtooth wave signal v_{ramp} to generate the pulse width modulation (PWM) signal u. When $v_{con} > v_{ramp}$, S1 and S4 are on, and S2 and S3 are off. Meanwhile, when $v_{con} < v_{ramp}$, S2 and S3 are on, and S1 and S4 are off. Therefore, the driving waveforms of the switch tubes diagonally across from each other, such as S1 and S4, are identical, and the switching states of S1 and S2 are opposite. The state variables X in the equivalent circuit of an SS-type ICPT system are composed of inductor current and capacitor voltage, that is $X=[v_{cp}, v_{cs}, v_c, i_p, i_s, i_L]^T$. Since the eight switching devices in this system work in combination, the system has six switching states as shown in Table I.

The energy conversion link, including the inverter and rectification, exhibits hard switching nonlinearity. To describe the switching nonlinearity of the energy conversion link in an ICPT system, two nonlinear variables s and g are defined in Eqn. (2).

$$s = \begin{cases} 1 & i_s > 0 \\ -1 & i_s < 0 \end{cases} \qquad g = \begin{cases} 1 & v_{con} >= v_{ramp} \\ -1 & v_{con} < v_{ramp} \end{cases} \tag{2}$$

According to the ICPT system mutual inductance coupling model, the system state equation based on voltage loop control is established in Eqn. (3).

$$\dot{X} = A_i X + B_i E \tag{3}$$

where i (i=1, 2, 3, 4, 5, 6) corresponds to the six switching states of the system, and A_i and B_i are specifically defined in Eqns. (4)-(6).

$$A_i = \begin{bmatrix} 0 & 0 & 0 & \frac{1}{C_p} & 0 & 0 \\ 0 & 0 & 0 & 0 & \frac{1}{C_s} & 0 \\ 0 & 0 & \frac{-1}{RC} & 0 & 0 & \frac{1}{C} \\ \frac{L_s+L}{\Delta} & \frac{M}{\Delta} & \frac{sM}{\Delta} & \frac{(L_s+L)R_p}{\Delta} & \frac{MR_p}{\Delta} & 0 \\ \frac{M}{\Delta} & \frac{L_p}{\Delta} & \frac{sL_p}{\Delta} & \frac{MR_p}{\Delta} & \frac{L_pR_s}{\Delta} & 0 \\ \frac{sM}{\Delta} & \frac{sL_p}{\Delta} & \frac{L_p}{\Delta} & \frac{sMR_p}{\Delta} & 0 & \frac{sL_pR_s}{\Delta} \end{bmatrix} \quad s = \begin{cases} 1 & i = 1,4 \\ -1 & i = 2,3 \end{cases} \tag{4}$$

$$A_i = \begin{bmatrix} 0 & 0 & 0 & \frac{1}{C_p} & 0 & 0 \\ 0 & 0 & 0 & 0 & 0 & 0 \\ 0 & 0 & \frac{-1}{RC} & 0 & 0 & 0 \\ \frac{-1}{L_p} & 0 & 0 & \frac{-R_p}{L_p} & 0 & 0 \\ 0 & 0 & 0 & 0 & 0 & 0 \\ 0 & 0 & 0 & 0 & 0 & 0 \end{bmatrix} \quad i = 5,6 \tag{5}$$

$$B_i = \begin{bmatrix} 0 \\ 0 \\ 0 \\ -\frac{g(L_s+L)}{\Delta} \\ -\frac{gM}{\Delta} \\ -\frac{gM}{\Delta} \end{bmatrix} \quad g = \begin{cases} 1 & i = 1,2 \\ -1 & i = 3,4 \end{cases} \qquad B_i = \begin{bmatrix} 0 \\ 0 \\ 0 \\ \frac{g}{L_p} \\ 0 \\ 0 \end{bmatrix} \quad g = \begin{cases} 1 & i = 5 \\ -1 & i = 6 \end{cases} \tag{6}$$

When the system works in modes 1, 2, 3 and 4, i_s is not equal to zero, and it works in the Continuous Current Mode (CCM). When the system works in modes 5 and 6, i_s is equal to zero, and it works in the Discontinuous Current Mode (DCM).

III. ANALYSIS OF NONLINEAR PHENOMENA IN THE SYSTEM

Based on the mathematical model of an ICPT system established in section II, the nonlinear phenomena in an ICPT system is studied in this section from the perspective of

TABLE II
MAIN CIRCUIT PARAMETERS

Notation	Value
Input voltage E/V	30
Frequency f/kHz	10
Coil inductance L_p &L_s /uH	115
Compensation capacitor C_p & C_s /uF	2.2
Parasitic resistance R_p& R_s /Ω	0.15
Filter inductor L/mH	1.5
Filter capacitor C/ uF	220
Load Resistance R/Ω	10
Scale factor $G1$	0.6
Scale factor $G2$	0.4
Reference voltage v_{ref}/V	20
Upper saturation boundary value of $v$ref v_H/V	8
Lower saturation boundary value of $v$ref v_L/V	2
Coupling coefficient k	(0.2, 0.85)

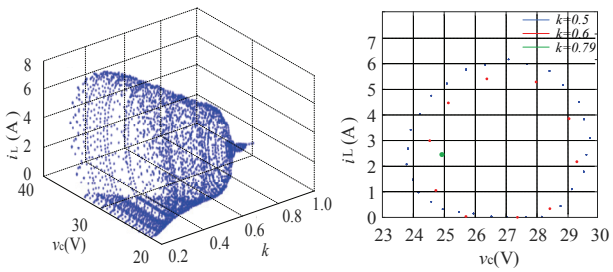

(a) (b)

Fig. 2. Bifurcation diagram with the coupling coefficient k as a bifurcation parameter. (a) Three-dimensional bifurcation diagram with the coupling coefficient k as a bifurcation parameter. (b) Poincare section diagram under typical coupling coefficients k.

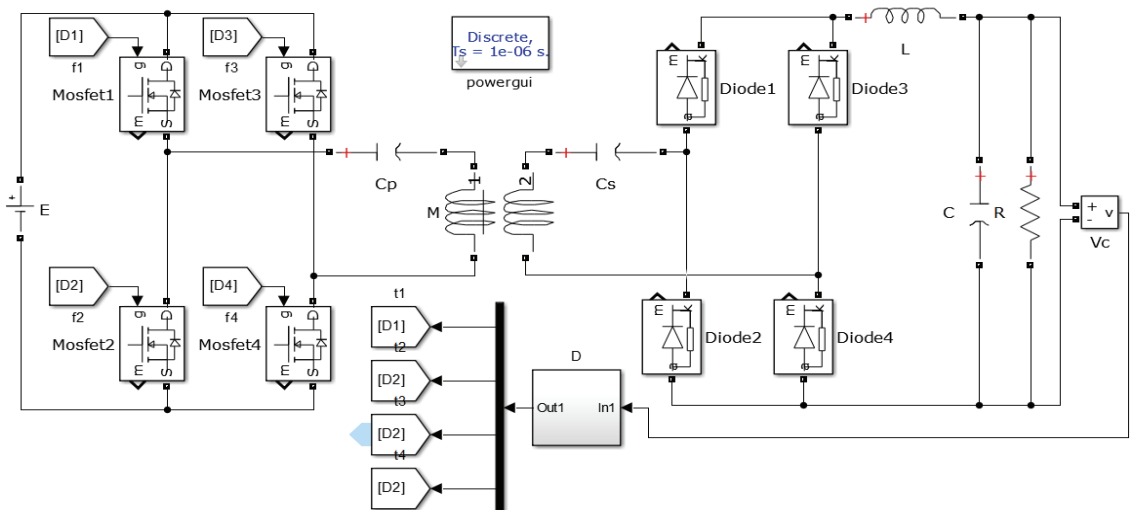

Fig. 3. Simulation diagram of an ICPT system based on SS-type compensation.

numerical simulation and theoretical modeling. Firstly, a three-dimensional bifurcation diagram with the coupling coefficient as the bifurcation parameter is established with a numerical simulation to observe the influence of the coupling coefficient on the stability of an ICPT system. Then a Jacobian matrix model is deduced with discrete mapping numerical modeling and Filippov's method to determine the stability of the system periodic closed orbit. Finally, the modeling results are compared with the numerical simulation results to verify the correctness of the model.

A. Numerical Simulation

In order to analyze the nonlinear phenomena in an ICPT system, the system parameters are shown in Table II. A large value of the filter inductance value is taken here to observe the influence of the filter inductor on the nonlinear phenomena in an ICPT system under different coupling conditions.

Numerical simulations are carried out based on Eqns. (3)-(5).The system bifurcation diagram, shown in Fig. 2(a), takes the coupling coefficient k as the bifurcation parameter. In Fig. 2, v_c is the output voltage after the n^{th} iteration, and i_L is the filter inductor current after the n^{th} iteration.

Furthermore, the simulation diagram shown in Fig. 3 and the system parameters shown in Table II are adopted to simulate the working condition of a system under different coupling coefficient in MATLAB/Simulink.

It can be seen from Fig. 2(a) that when the coupling coefficient k is not less than 0.79, the system works in the stable state. Meanwhile, when k is between 0.6 and 0.79, a low-frequency oscillation whose frequency is much smaller than the switching frequency occurs in the system. Furthermore, when k is less than 0.6, the duty ratio reaches the lower limit of saturation, the degree of severe toroidal ruptures and a boundary collision occurs. Therefore, k=0.79 is the stable operating boundary of the system, and k=0.6 is the boundary where a boundary collision occurs. To clearly describe the system operating status, Fig. 2(b) shows a sampling phase diagram (Poincare section diagram) under typical coupling coefficients of 0.79, 0.6 and 0.5, where k=0.5 is chosen to show that the phenomenon of a low-frequency oscillation in

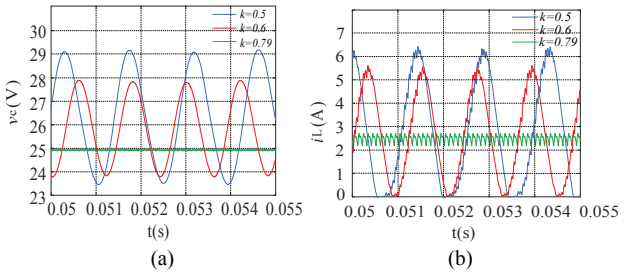

Fig. 4. Circuit simulation waveforms under typical coupling coefficient k. (a) Waveforms of v_c. (b) Waveforms of i_L.

the system is intensified with a decreased coupling coefficient k. Therefore, k=0.79, 0.6 and 0.5 are chosen as typical coupling coefficients to study the nonlinear behavior in the system.

Simulation results are shown in Fig. 4. Waveforms of the output voltage and filter inductor current under typical coupling coefficient are shown in Fig. 4(a) and Fig. 4(b), respectively.

It can be clearly seen from Fig. 2 and Fig. 4 that the specific process of the system state changing with decreases of the coupling coefficient k is described as follows.

When k is between 0.79 and 0.85, the system works in the cycle one orbit, and the sequence of the states for the switching cycle is 1→2→3→4→1.

When k is between 0.6 and 0.78, a low-frequency oscillation phenomenon occurs at the filter inductor current and output voltage. The frequency of the oscillation is about one percent of the switching frequency. A Poincare section of the system is distributed in a ring. According to the nonlinear dynamics theory [18], the system is in a quasi-periodic state and generates low-frequency bifurcation.

When k is less than 0.6, the system continues working in an unstable state, the duty ratio reaches the lower limit of saturation, the degree of low-frequency oscillation is deepened, the phenomena of severe toroidal rupture and boundary collision occurs. At this time, the ripples of v_c and i_L reach 6V and 8A, respectively. In addition, the system enters the DCM mode.

B. Modeling and Stability Analysis of the System

It can be seen from section IIIA that an ICPT system generates the phenomenon of a low-frequency oscillation when the coupling coefficient is less than 0.79. Therefore, this section theoretically models the system and analyzes the causes of the oscillations. Firstly, the system is analyzed with discrete mapping numerical modeling and Filippov's method to deduce a Jacobian matrix model. Discrete mapping numerical modeling can be adopted to analyze the dynamic behavior of the switching frequency scale of the system and to determine the stability of the system since it is completely closed to actual circuit system operation. Filippov's method, which has been commonly applied to mechanical switching systems, can be used fruitfully in power electronic circuits to describe the nonlinear behavior of the system during switchings. It is possible to describe the stability of power electronic converters by combining Filippov's method and Floquet theory. Then the eigenvalue of a Jacobian matrix is calculated to predict the boundary of stable operation and the position of the bifurcation point of the system. Finally, the established Jacobian matrix model lays the foundation for the parameters design process of the system.

The status equations of the system have been established according to the analysis in section II. The following adopts sawtooth periodic sampling to construct the model, where i (i=1, 2, 3, 4, 5 and 6) correspond to the six kinds of switch states of the system. To simplify the modeling results, the state differential equation is constructed as Eqn. (7).

$$\dot{X} = f(X(t_i),t) = e^{A_i t_i} X(t_i) + (e^{A_i t_i} - \mathrm{I}) A_i^{-1} B_i E \tag{7}$$

where , $t_i = d_i T$, t_i represents the time of each state, $X(t_i)$ represents the state variable of the system at different switch states, and I represents the six-order unit array.

Simplifying Eqn. (7) yields:

$$P_i = e^{A_i t_i}, p_i = \begin{cases} (e^{A_i t_i} - \mathrm{I}) A_i^{-1} B_i E, & i = 1,2,3,4; \\ t_i B_i E, & i = 5,6. \end{cases} \tag{8}$$

The iterative equation is constructed as Eqn. (9).

$$X_{n+1} = \prod_{i=1}^{6} P_i X_n + \prod_{i=2}^{6} P_i p_1 + \prod_{i=3}^{6} P_i p_2 + \prod_{i=4}^{6} P_i p_3 + \prod_{i=5}^{6} P_i p_4 + P_6 p_5 + p_6 \tag{9}$$

The fixed point X_Q represents the state variable of the system working in the steady state, and the switching point X_{Di} represents the state variable of the system at the time of switching. The calculations of X_Q and X_{Di} are obtained by Eqn. (10).

$$X_{Di} = P_i X_Q + p_i, X_Q = (\mathrm{I} - \prod_{i=1}^{4} P_i)^{-1} (\prod_{i=2}^{4} P_i p_1 + \prod_{i=3}^{4} P_i p_2 + P_4 p_3 + p_4) \tag{10}$$

When the system works in a stable cycle one state, the fixed point X_Q of Eqn. (10) is stable. At this time, the switching order of the system state is 1→2→3→4→1. To calculate the time of each state in one switching cycle, the switching conditions are deduced by the values of u_c and i_L at the moment of switching as follows:

$$h_i = \begin{cases} v_{\mathrm{ref}} / G_1 + F_i & i = 1,3,4 \\ \left(v_{\mathrm{L}} + (v_{\mathrm{H}} - v_{\mathrm{L}}) \cdot \sum_{i=1}^{2} d_i\right) / G_1 / G_2 + F_i & i = 2 \\ \left(v_{\mathrm{L}} + (v_{\mathrm{H}} - v_{\mathrm{L}}) \cdot \sum_{i=1}^{5} d_i\right) / G_1 / G_2 + F_i & i = 5 \\ F_i = \mathrm{equ}_i \cdot XD_i - v_{\mathrm{ref}} / G_1 \end{cases} \tag{11}$$

where h_i represents the condition change from state i to state i+1, $n_1 = n_3 = n_4 = (0,0,0,0,1,0)$ $n_2 = n_5 = (0,0,-G_1G_2,0,0,0)$. In addition, G_1, G_2, v_H and v_L have already been defined in Table II.

According to Filippov's method, the discrete Jacobian matrix can be expressed as Eqn. (12).

$$J = J_4 S_3 J_3 S_2 J_2 S_1 J_1 \tag{12}$$

TABLE III
MAXIMUM EIGENVALUE OF JACOBIAN MATRIX CHANGES WITH THE PARAMETER K

Coupling coefficient k	Maximum feature multiplier	System status
0.83	0.9196±0.3467j	Stable
0.82	0.9239±0.3462j	Stable
0.81	0.9286±0.3458j	Stable
0.80	0.9320±0.3455j	Stable
0.79	0.9379±0.3451j	Stable
0.78	0.9431±0.3444j	Hopf bifurcation
0.77	0.9487±0.3438j	Low frequency oscillation

where $J_1 = e^{A_1 d_1 \mathrm{T}}$ $J_2 = e^{A_2 d_2 \mathrm{T}}$ $J_3 = e^{A_3 d_3 \mathrm{T}}$ $J_4 = e^{A_4 d_4 \mathrm{T}}$. In addition, S_i represents the jump matrix, which can be obtained as follows:

$$S_i = \mathrm{I} + \frac{(X_{\mathrm{D}(i+1)} - X_{\mathrm{D}i}) n_i}{n_i X_{\mathrm{D}(i+1)} + \left.\frac{\partial h_i}{\partial t}\right|_{t=t_\Sigma}} \quad t_\Sigma = \sum_{j=1}^{i} t_j \quad i = 1,2,3,4;$$

where $X_{\mathrm{D}(i+1)}$ represents the state variable of the next switching moment.

According to Floquet theory, the stability of the periodic closed-loop is depend on the maximum of Jacobian matrix's eigenvalues. In addition, the characteristic equation defined by Floquet theory can be expressed as Eqn. (13).

$$\det(\lambda \mathrm{I} - J) = 0 \tag{13}$$

According to the numerical simulation results, the phenomenon of a low-frequency oscillation occurs around k=0.78. Therefore, the eigenvalues of the Jacobian matrix of the system are specially analyzed around the coupling coefficient k=0.78. The maximum of the eigenvalues under different coupling coefficients are shown in Table III.

It is shown in Table III that when the coupling coefficient k, which is the bifurcation parameter, is not less than 0.79, the Jacobin matrix eigenvalues at the fixed point X_Q are located within the unit circle. This means that the system works in a stable domain. Then the maximum eigenvalue of the Jacobian matrix crosses out of the unit circle along the complex plane with a decrease of the coupling coefficient k. This indicates that Hopf bifurcation occurs in the system at this time. According to the authors of [20], when Hopf bifurcation occurs in a system, the periodic fixed point of the system loses its stability and the motion of the system changes from a fixed point to a limit cycle. In addition, the state variable of the system generates a low-frequency oscillation. This low frequency oscillation increases both the ripple of the system output and the system switching stress, which results in increased losses and reduced performance.

According to the above analysis, the phenomenon of a low-frequency oscillation in the system is caused by Hopf bifurcation. At the same time, according to the authors of [19],

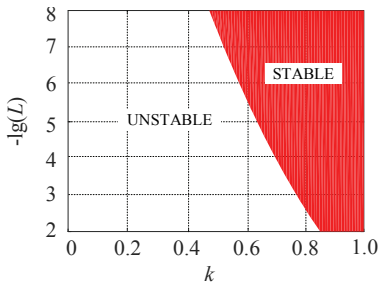

Fig. 5. Stable domain of the system.

different values of the parameter affect the stable operation of the system and cause nonlinear phenomena in the system. In order to clearly observe this nonlinear phenomenon, the value of the filter inductor is made extremely large, which is quite different from actual operation.

Therefore, the coupling coefficient and the filter inductance are studied as variables to observe the influence of the filter inductor value on the nonlinear behavior of the system under different coupling conditions. The value of the filter inductor is made to range from 10nH to 10mH.

According to Eqn. (12), the eigenvalues of the Jacobian matrix are calculated by MATLAB. In the parameter domain shown in Fig. 5, the points whose eigenvalues lying in the unit circle are shown in the shaded part of the figure. The shaded part constitutes the stable domain of the parameter.

It can be seen from Fig. 5 that the stability range of the system in $k \in (0,1)$ decreases with an increase of the filter inductance value. This indicates that although different values of the filter inductance affect the position of the bifurcation point of the system, the Hopf bifurcation phenomenon does not disappear with a decrease of the filter inductance value. Therefore, the value of the filter inductance does not affect the analysis of the Hopf bifurcation phenomenon.

Thus, a method of suppressing the Hopf bifurcation phenomenon is studied by analyzing the other parameters in the system.

IV. METHOD OF ICPT SYSTEM PARAMETER DESIGN

The numerical simulation in section IIIA verifies that the ICPT system generates a low-frequency oscillation when a nonlinear switching device is working and the parameter selection is unreasonable. The eigenvalues of the Jacobian matrix model, deduced through theoretical modeling in section IIIB, determine the stability of the system periodic closed orbit. According to the analysis above, when the coupling coefficient is lower than 0.79, the system enters an unstable state and the stability domain is small. In addition, the system circuit structure and main circuit parameters have been determined. Therefore, a parameter design method is proposed here to make a system under the weak coupling condition work in the stable state by modifying the feedback loop proportional coefficients G_1 and G_2 without changing

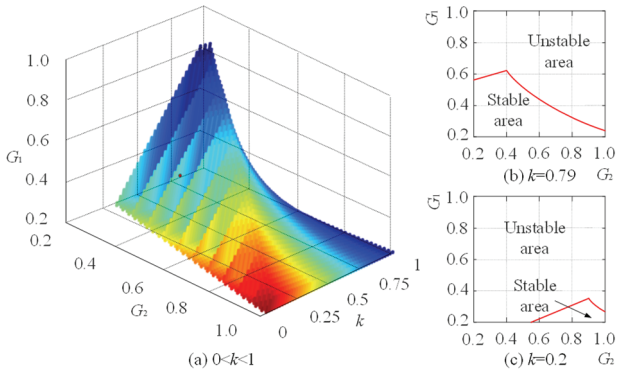

Fig. 6. Stable domain of filter inductor current. (a) Stable domain in the G_1-G_2-k phase space. (b) Stable domain in G_1-G_2 under k=0.79. (c) stable domain in G_1-G_2 under k=0.2.

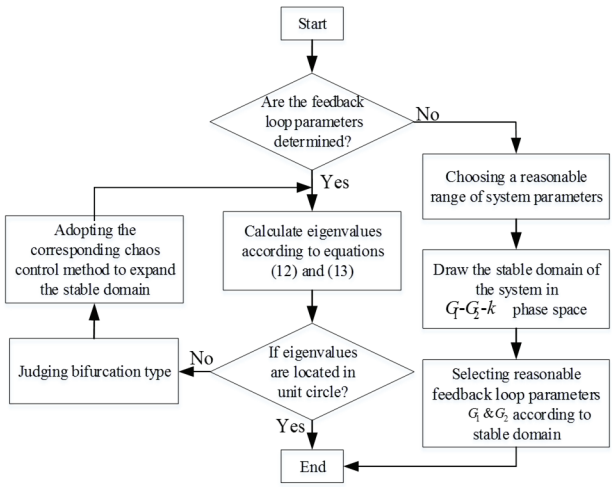

Fig. 7. Flow chart of the proposed parameter design based on the stability principle for an ICPT system.

the structure or main circuit parameters of the system. The parameters G_1 and G_2 can be determined by the stable domain of the system, which are calculated by a combination of Eqns. (10)-(12).

As shown in Fig. 6(a), the stable domain (shaded part) is obtained by a MATLAB numerical simulation with the parameters shown in Table II, where G_1=0.6 and G_2=0.4. It should be noted that the color of the graph has no practical meaning. Fig. 6(b) shows the stable interval of the filter inductor current in the G_1-G_2 region under k=0.79. In addition, the system works in the stable domain at this time. Fig. 6(c) shows the stable interval with k=0.2. The system is unstable at this time. Consequently, according to the conclusions above, which are consistent with the numerical simulation, it is possible to change the feedback loop proportional coefficient as G_1=0.22 and G_2=0.81 to make the system work in the stable state under weak coupling conditions.

When the ICPT system is designed, the circuit parameters such as the self-inductance, mutual inductance, compensation capacitance, filter inductance, filter capacitor, etc. of the main circuit can be determined according to the actual situation. However, the feedback loop parameters are not easily determined. The parameter design method proposed here can be realized by modifying the feedback loop parameters or by adopting other control methods to achieve stable operation of the system within certain parameters (such as a low coupling coefficient). Therefore, the specific parameter design flow of an ICPT system is shown in Fig. 7.

To ensure that the system can work stably under certain conditions, the uncertain parameters, such as the feedback loop parameters, can be chosen from the stable interval, which is obtained by the numerical simulations of Eqns. (10)-(12) based on a MATLAB simulation according to the theoretical analysis in section IIIA. Since it is impossible to change the determined parameters such as the main circuit parameters, the system is forced into the stable state by adopting corresponding control methods, which include the time delay feedback control strategy, the PID nonlinear control strategy, the self-stabilizing chaos control strategy, etc. However, the system characteristics at this time are also changed too. Thus, no detailed study is done here.

V. Experimental Verification

In order to verify the correctness of the above nonlinearity analysis, a system experimental platform with an inverter operating frequency of 10kHz is built, as shown in Fig. 8, based on the circuit structure of Fig. 1 and the parameters in Table II. The state variables of the system under typical coupling coefficients are observed to verify the correctness of both the simulation and the modeling. In the experimental platform, the output voltage v_c is sampled by the voltage sampling module based on Hall sensors. In order to simplify the experimental process, the voltage sampling signal is directly fed back to the DSP to generate the pulse modulation signal of the switching tube.

A phase diagram is drawn to replace the Poincare section since Poincare sections are difficult to obtain during experiments. Fig. 9, Fig. 10 and Fig. 11 show experimental waveforms of the system with coupling coefficients of 0.79, 0.6 and 0.5, respectively. Fig. 9(a), Fig. 10(a) and Fig. 11(a) represent phase diagrams of v_c and i_L. Fig. 9(b), Fig. 10(b) and Fig. 11(b) show waveforms of the output voltage v_c, with time intervals of 50us, 1ms and 500us, respectively. Fig. 9(c), Fig. 10(c) and Fig. 11(c) show waveforms of the filter inductance current i_L, with time intervals of 50us, 500us and 500us, respectively. In addition, Simulink/FFT is used to analyze various oscillation frequencies of i_L in the system under different coupling coefficients, and they are shown in Fig. 9(d), Fig. 10(d) and Fig. 11(d).

It can be seen from Fig. 9 that the system works in the stable state with k=0.79. It can also be seen that the output voltage is 24V, the output voltage ripple is small, less than 1%, and the inductor current ripple is small, 1A. According to Fig. 9(d), the main harmonic frequency is 10kHz. The quantization error

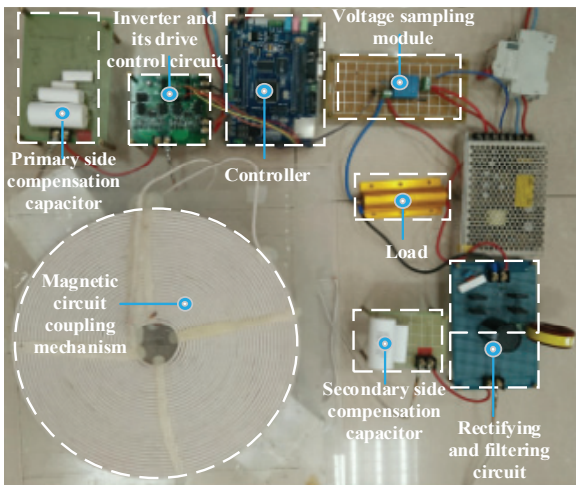

Fig. 8. Experimental platform of the system.

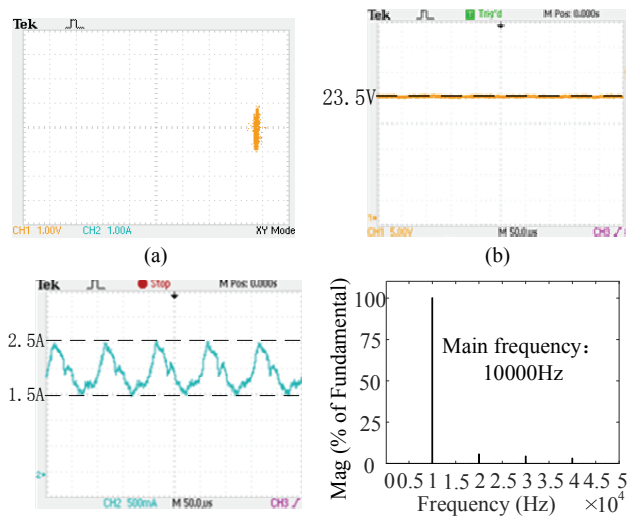

Fig. 9. Experimental waveforms of the system with k=0.79. (a) Phase diagram of i_L-v_c. (b) Time domain diagram of v_c. (c) Time domain diagram of i_L. (d) Results of a FFT analysis of i_L.

of the sampling, digital calculation and PWM link are the main reasons for the increase of the experimental waveform ripple.

According to Fig. 10, when k decreases to 0.6, waveforms of v_c and i_L oscillate at a low frequency. Fig. 10(a) shows that the limit loop oscillates at this time. According to Fig. 10(b) and Fig. 10(c), the average of the output voltage decreases to 22.5V, the voltage ripple is 5V, and the current ripple is 5A. The system generates low-frequency oscillation phenomena at this point, and the frequency of the oscillation is about one eighth the switching frequency, which is roughly the same as the result of Fig. 10(d).

According to Fig. 11, when k decreases to 0.5, the inductor current decreases to zero, the limit cycle oscillates severely, the torus enlarges. In addition, boundary collision and severe toroidal rupture occur. The system enters the DCM mode. The ripples of v_c and i_L are 8V and 7.2A. respectively. In addition, the low-frequency oscillation of the system becomes

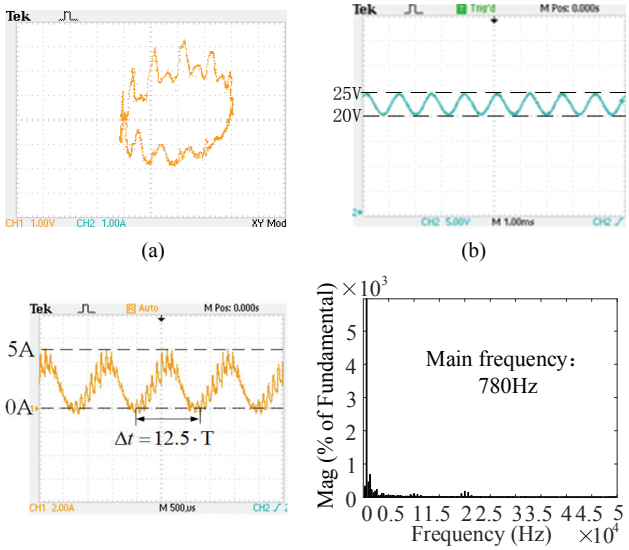

Fig. 10. Experimental waveforms of the system with k=0.6. (a) Phase diagram of i_L-v_c. (b) Time domain diagram of v_c. (c) Time domain diagram of i_L. (d) Results of a FFT analysis of i_L.

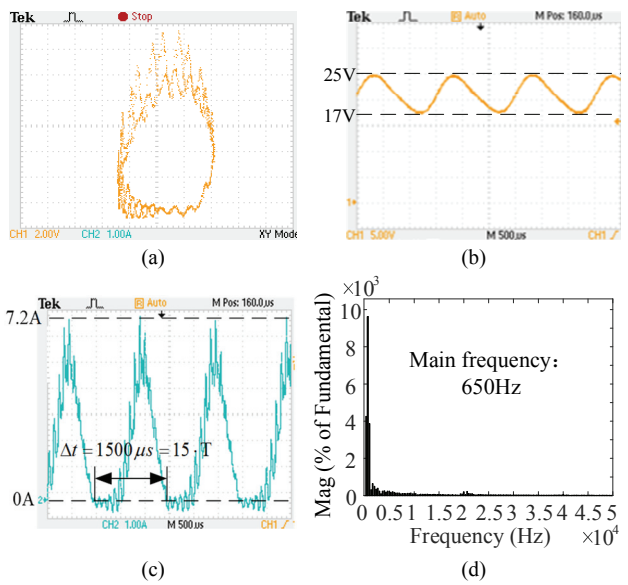

Fig. 11. Experimental waveforms of the system with k=0.5. (a) Phase diagram of i_L-v_c. (b) Time domain diagram of v_c. (c) Time domain diagram of i_L. (d) Results of a FFT analysis of i_L.

more serious. The frequency of the oscillation is about one-fifteenth that of the switching frequency, which is roughly the same as the result of Fig. 11(d).

According to the analysis in section IV, the feedback loop proportional coefficients G_1=0.22 and G_2=0.81 can be changed to make the system work in the stable state when k=0.2.

Therefore, an experiment is carried out to verify its correctness with the parameters k=0.2, G_1=0.22 and G_2=0.81. Waveforms of the output voltage v_c and the filter inductance current i_L are given in Fig. 12.

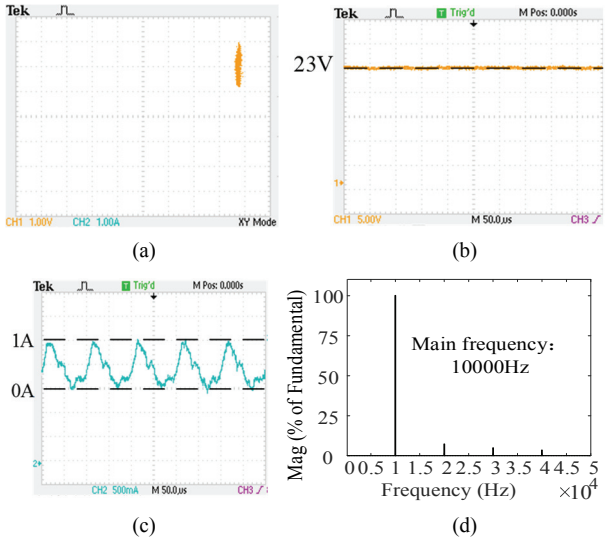

Fig.12. Experimental waveforms of the system with k=0.2, G_1=0.22 and G_2=0.81. (a) Phase diagram of i_L-vc. (b) Time domain diagram of vc. (c) Time domain diagram of i_L. (d) Results of a FFT analysis of i_L.

It can be seen from Fig. 12 that the system can still work in the stable state with k=0.2, G_1=0.22 and G_2=0.81, which is consistent with the simulation results.

According to the experimental results above, it can be seen that improper design of the system parameters results in Hopf bifurcation of a system under weak coupling conditions. It can also be seen that Hopf bifurcation generates low-frequency oscillation of the system. Experimental waveforms of v_c and i_L correspond to the simulations, which further verified the correctness of the numerical simulation and theoretical modeling.

VI. Conclusion

In order to study the Hopf bifurcation in ICPT systems, discrete mapping numerical modeling and Filippov's method are adopted to deduce a Jacobian matrix model, whose eigenvalues determine the boundary of the stable operation of the system. Then the general flow of the parameter design is proposed based on the stability principle of an ICPT system. This is done to realize stable operation under the condition of a weak coupling by changing the feedback loop parameters. The modeling can do a good job of describing the evolution of the system's transient behavior. In addition, it has value for the study of the low-frequency oscillation behavior and parameter design of ICPT systems. Finally, an experimental platform is built to verify the correctness of the numerical simulation and modeling.

However, the shortcoming of this paper is that the control method adopted in this paper is a PWM control method, which may cause some undesirable issues, such as the loss of ZVS operation. In this case, a low resonant frequency of 10 kHz is used in this paper to reduce the switching loss. Therefore, other control methods, such as the phase shift control method need to be studied in the future.

Acknowledgment

This work was supported by the National Natural Science Foundation of China (Grant no. 51777210), the Jiangsu Natural Science Foundation (Grant no. BK20171190) and the Xuzhou Science and Technology Project (Grant no. KC18104).

References

[1] I. Mayordomo, T. Dräger, P. Spies, J. Bernhard, and A. Pflaum, "An overview of technical challenges and advances of inductive wireless power transmission," *Proceedings of the IEEE*, Vol. 101, No. 6, pp. 1302-1311, 2013.

[2] S.-Y. Ren, C.-Y. Xia, L.-M. Liu, X.-J. Wu, and Q. Yu, "Cross-shaped magnetic coupling structure for electric vehicle IPT charging systems," *J. Power Electron.*, Vol. 18, No. 4, pp. 1278-1292, Jul. 2018.

[3] Q. Ke, P.-P. Jiang, and G.-Z. Yan, "Standardized design of the transmitting coils in inductive coupled endoscope robot driving systems," *J. Power Electron.*, Vol. 17, No. 3, pp. 835-847, May 2017.

[4] L. Chen, Y.-G. Su, Y.-M. Zhao, C.-S. Tang, and X. Dai, "Load and mutual inductance identification method for series-parallel compensated IPT systems" *J. Power Electron.*, Vol. 17, No. 6, pp. 1545-1552, Nov. 2017.

[5] Q. Xu, H. Wang, Z. Gao, Z. Mao, J. He, and M. Sun, "A novel mat-based system for position-varying wireless power transfer to biomedical implants," *IEEE Trans. Magn.*, Vol. 49, No. 8, pp. 4774-4779, Aug. 2013.

[6] A. Berger, M. Agostinelli, C. Sandner, S. Vesti, and M. Huemer, "High efficient integrated power receiver for a Qi compliant wireless power transfer system," *Wireless Power Transfer Conference. IEEE*, pp. 1-4, 2016.

[7] M. Park, V. T. Nguyen, S.-D. Yu, S.-W. Yim, K. Park, B. D. Min, S.-D. Kim, and J. G. Cho, "A study of wireless power transfer topologies for 3.3 kW and 6.6 kW electric vehicle charging infrastructure," *Transportation Electrification Asia-Pacific. IEEE*, pp. 689-692. 2016.

[8] B. Esteban, M. Sid-Ahmed, and N. C. Kar, "A comparative study of power supply architectures in wireless EV charging systems," *IEEE Trans. Power Electron.*, Vol. 30, No. 11, pp. 6408-6422, Nov. 2015.

[9] X. Dai, X.-Y. Huang, and Y. Sun, "Study on discrete time mapping modeling and stability analysis for piecewise autonomous oscillation systems," *Acta Automatica Sinica,* Vol. 33, No. 1, pp. 72-77, Jan. 2007.

[10] F. Xie, B. Zhang, and D.-Y. Qiu, "Nonlinear behaviors analysis of full-bridge resonant converter based on loosely coupled transformer," *Automation of Electric Power Systems*, Vol. 38, No. 3, pp. 47-51, Feb. 2014.

[11] X.-M. Chen, W.-Q. Niu, and X. Zhang, "Design and implement of a high-frequency bridge type AC-AC direct converter for contactless power transfer systems," *Electrical Power Systems and Computers. Springer Berlin Heidelberg*, pp. 139-146, 2011.

[12] R.-K. Mai, T.-R. Lin, Y. Li, and Z.-Y. He, "Study on small signal modeling and controlling for dual transmitters based inductive power transfer system," *Proceedings of the Csee*, Vol. 37, No. 20, pp. 6068-6076, 2017.

[13] B. Zhang and H. Li, "Application for color matching in textile dyeing based on numerical analysis," *International Conference on Computer Science and Software Engineering. IEEE Computer Society*, pp. 357-360, 2008.
[14] A. P. Hu, "Modeling a contactless power supply using GSSA method," *IEEE International Conference on Industrial Technology. IEEE*, pp. 1-6, 2009.
[15] H. H. C. Iu and C. K. Tse, "Study of low-frequency bifurcation phenomena of a parallel-connected boost converter system via simple averaged models," *IEEE Trans. Circuits Syst. L Fundam. Theory Appl*, Vol. 50, No. 5, pp. 679-685, May 2003.
[16] D. Giaouris, S. Banerjee, B. Zahawi, and V. Pickert, "Control of fast scale bifurcations in power-factor correction converters," *IEEE Trans. Circuits Syst.*, Vol. 54, No. 9, pp. 805-809, Sep. 2007.
[17] F. Wang, H. Zhang, and X. Ma, "Analysis of slow-scale instability in boost PFC converter using the method of harmonic balance and floquet theory," *IEEE Trans. Circuits Syst. I Reg. Papers*, Vol. 57, No. 2, pp. 405-414, Feb. 2010.
[18] Y. Shi, Z.-J. Wu, X.-B. Dou, and M.-Q. Hu, "Research on bifurcation behaviors of three-phase full bridge inverters," *Proceedings of the Csee*, Vol. 36, No. 19, pp. 5334-5349+ 5416, 2016.
[19] D. Giaouris, S. Banerjee, B. Zahawi, and V. Pickert, "Stability analysis of the continuous conduction mode buck converter via Filippov's method", *IEEE Trans. Circuits Syst. I*, Vol. 55, pp. 1084-1096, May 2008.
[20] C. K. Tse, Y. M. Lai, and H. H. C. Iu, "Hopf bifurcation and chaos in a free-running current-controlled Cuk switching regulator," *IEEE Trans. Circuits Syst. I: Fundam. Theory Appl.*, Vol. 47, No. 4, pp. 448-457, Apr. 2000.

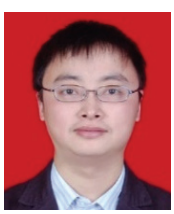

Chenyang Xia was born in Jiangsu Province, China, in 1982. He received his B.S., M.S. and Ph.D. degrees in Control Theory and Control Engineering from Chongqing University, Chongqing, China, in 2006, 2008 and 2010, respectively. From August 2018 to August 2019 he was an Academic Visitor at the University of Auckland, Auckland, New Zealand. He is presently working as an Associate Professor in the School of Electrical and Power Engineering, China University of Mining and Technology, Xuzhou, China. His current research interests include wireless power transfer and intelligent control.

Ying Yang was born in Jiangsu Province, China, in 1994. She received her B.S. degree in Electrical Engineering and Automation from the Nanjing University of Information Science and Technology, Jiangsu, China, in 2017. She is presently working towards her M.S. degree in the School of Electrical and Power Engineering, China University of Mining and Technology, Xuzhou, China. Her current research interests include wireless power transfer and its application.

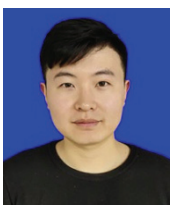

Yuxiang Peng was born in Jiangsu Province, China, in 1994. He received his B.S. degree in Electrical Engineering and Automation from Henan Polytechnic University, Jiaozuo, China, in 2017. He is presently working towards his M.S. degree in the School of Electrical and Power Engineering, China University of Mining and Technology, Xuzhou, China. His current research interests include wireless power transfer and its application.

Aiguo Patrick Hu received his B.S. and M.S. degrees from Xian Jiaotong University, Xian, China, in 1985 and 1988, respectively. He received his Ph.D. degree from the University of Auckland, Auckland, New Zealand, in 2001. He was a Lecturer and a Director of the China Italy Cooperative Technical Training Center, Xian, China; and the General Manager of a technical development company funded by the Asian2000 Foundation. He was with the National University of Singapore, Singapore, for a semester as an exchange Postdoctoral Research Fellow. He is currently in the Department of Electrical and Computer Engineering, University of Auckland. He is also the Head of Research of PowerbyProxi, Ltd. He holds 15 patents in wireless/contactless power transfer and microcomputer control technologies. He has published more than 200 papers in peer-reviewed journal and conference proceedings, authored a monograph on wireless inductive power transfer technology, and contributed four chapters to books.